

Quantum nondemolition measurement of a single electron spin in a quantum dot

Mitsuro Sugita*, Susumu Machida, Yoshihisa Yamamoto

Quantum Entanglement Project, ICORP, JST and Edward L. Ginzton Laboratory, Stanford University, Stanford, California 94305

(November 11, 2018)

We propose a scheme for the quantum nondemolition (QND) measurement of a single electron spin in a single quantum dot (QD). Analytical expressions are obtained for the optical Faraday effect between a quantum dot exciton and microcavity field. The feasibility of the QND measurement of a single electron spin is discussed for a GaAs/AlAs microcavity with an InAs QD.

I. INTRODUCTION

The measurement of a single electron spin in a semiconductor QD is of great importance, because an electron spin in a QD is proposed to be a key element to construct new optical and electronic devices, including a spin-based quantum computer [1,2]. A long decoherence time of the electronic spin is vital, but no experimental result for the lifetime of a truly single electron spin in a single QD has been reported so far, due to the lack of capability of measuring a single electron spin non-destructively.

Photoluminescence (PL) measurement has been used to access an individual QD [3,4]. Since PL measurement is a destructive process in a sense that real excitation and recombination of an electron-hole pair is involved, it is impossible to monitor a single electron spin non-destructively and continuously for a certain period of time. An alternative method, time-resolved Faraday rotation (TRFR) has been developed [5], which enables one to monitor the spin continuously, but a single spin measurement sensitivity has not been achieved yet [6,7].

In this paper, we propose an optical readout method based on the interaction between a single electron spin in a single QD and microcavity field, which enables us to perform QND monitoring of a single spin. In the proposed system, the phase shift of the probe light incurred by a single spin is enhanced by a microcavity. The coupled cavity-QD system is formulated by the quantum Langevin equations, and the response of the input probe light is analyzed quantitatively. It is shown that the polarization-sensitive Mach-Zehnder interferometer operating at the standard-quantum-limit can perform the QND measurement of a single electron spin, if the QD is incorporated into a high-Q microcavity or photonic bandgap structure.

This proposal is motivated by the recent experimental demonstration of a GaAs/AlAs DBR post-microcavity with a single InAs QD and an optical mode volume of $\sim (\lambda/n)^3$ [8] and theoretical prediction that such a microcavity should have a Q-value of higher than 10^4 [9].

II. SYSTEM CONFIGURATION

Figure 1 shows essential components of the scheme. (a) is the sample which consists of an InAs QD and GaAs/AlAs micropost cavity, and (b) and (c) are the electronic states and their coupling to the probe light (microcavity field). Suppose incident probe light traveling along z-axis has a linear polarization along x-axis. The polarization state can be decomposed into right and left circular polarizations, which we denote by the subscripts R and L respectively;

$$A_{in} = \begin{pmatrix} 1 \\ 0 \end{pmatrix} = \frac{1}{2} \begin{pmatrix} 1 \\ i \end{pmatrix} + \frac{1}{2} \begin{pmatrix} 1 \\ -i \end{pmatrix} = A_R + A_L. \quad (1)$$

If the sample has circular-birefringence, and the reflection coefficients are r_R and r_L , respectively, the reflected probe light field is

$$\begin{aligned} A_{out} &= r_R A_R + r_L A_L \\ &= \frac{1}{2} \begin{pmatrix} r_R + r_L \\ i(r_R - r_L) \end{pmatrix} = \begin{pmatrix} A_x \\ A_y \end{pmatrix}. \end{aligned} \quad (2)$$

In Fig. 1(b) and (c), the four different QD energy states, ground state electron and hole states with opposite spins, and their coupling to probe light with two circular polarizations, R and L , are shown. The conduction band ground

state of the QD is the angular momentum state of $\pm 1/2$, and the valence band ground state is that of $\pm 3/2$, if we neglect the heavy hole and light hole band mixing effect. Because of the selection rule, which defines allowed and forbidden transitions in the electric dipole approximation, the up-spin channel only couples to L polarization and the down-spin does to R polarization. r and r_0 are the responses of the QD system to the probe light for the allowed and forbidden channels, respectively.

The y-component of the reflected probe light for the two cases in Fig. 1(b) (up-spin) and (c) (down-spin) are

$$A_y = \begin{cases} +\frac{i}{2}(r - r_0) & \text{for up-spin} \\ -\frac{i}{2}(r - r_0) & \text{for down-spin} \end{cases} \quad (3)$$

If we introduce the amplitude and the phase responses for the two polarizations separately, as $r_{R,L} = |r_{R,L}|e^{i\theta_{R,L}}$, via

$$\begin{aligned} \bar{r} &\equiv \frac{|r_R| + |r_L|}{2}, \quad dr \equiv |r_R| - |r_L|, \\ \bar{\theta} &\equiv \frac{\theta_R + \theta_L}{2}, \quad d\theta \equiv \theta_R - \theta_L, \end{aligned} \quad (4)$$

the reflected probe amplitude is represented in first order of dr and $d\theta$ as,

$$A_{out} = \bar{r}e^{i\bar{\theta}} \left(-\frac{d\theta}{2} - i\frac{dr}{2\bar{r}} \right). \quad (5)$$

We use a dispersive regime with negligible real excitation, so, $d\theta \gg dr/\bar{r}$. The linearly polarized light is obtained as an output with a slight rotation proportional to the difference of the phase between the two circular polarizations. This rotation corresponds to a simple magneto-optical Faraday effect by a single spin. The signal is

$$A_y = \begin{cases} +\frac{\theta - \theta_0}{2}\bar{r}e^{i\bar{\theta}} & \text{for up-spin} \\ -\frac{\theta - \theta_0}{2}\bar{r}e^{i\bar{\theta}} & \text{for down-spin} \end{cases}, \quad (6)$$

where $\theta \equiv \text{Arg}(r)$ and $\theta_0 \equiv \text{Arg}(r_0)$.

In Fig. 2, the responses θ and θ_0 , with and without the QD electron spin, are shown as a function of the probe light frequency detuning from the QD transition frequency. One can measure the signals in Eq.(6) using a polarization sensitive interferometer shown in Fig. 3. Details of the responses and the setup are described in the following sections.

III. EXPECTED PHASE ROTATION

In this section, we derive the responses r and r_0 of an optical microcavity with and without photon-exciton coupling. Figure 4 shows a mathematical model, where three systems couple with each other by the coupling constants, γ_p , Ω , γ_{ex} . For simplicity, we assume the cavity is single-sided, i.e., the second mirror is perfect. The reason for introducing a microcavity is that the Faraday effect of a single spin would be small and need to be enhanced by the photon storage effect of the cavity.

The Hamiltonian for our system is

$$H = H_p + H_{ex} + H_{res} + H_{p-ex} + H_{p-res}, \quad (7)$$

where

$$H_p = \hbar\omega_p \sum_i a_i^\dagger a_i, \quad H_{ex} = \frac{\hbar\omega_{ex}}{2} \sum_j \sigma_{zj}, \quad H_{res} = \int \hbar\omega \sum_i b_i^\dagger(\omega) b_i(\omega) d\omega,$$

$$H_{p-ex} = i\frac{\hbar}{2} \sum_{ij} (\Omega_{ij} a_i \sigma_{+j} - \Omega_{ij}^* a_i^\dagger \sigma_{-j}), \quad H_{p-res} = i\hbar \int \sum_{ii'} \kappa_{ii'}(\omega) (a_i^\dagger b_{i'}(\omega) - a_i b_{i'}^\dagger(\omega)),$$

where

$$\Omega_{ij} = \frac{2e}{\hbar} \sqrt{\frac{\hbar\omega_p}{2\epsilon V_{cav}}} < c_j | \frac{x \pm iy}{\sqrt{2}} | v_j > \quad (+ \text{ for } i = 1, - \text{ for } i = 2),$$

$$\sigma_{-j} = d_{vj}^\dagger d_{cj}, \quad \sigma_{+j} = d_{cj}^\dagger d_{vj}, \quad \sigma_{zj} = d_{cj}^\dagger d_{cj} - d_{vj}^\dagger d_{vj}, \quad (8)$$

under the rotating wave and the electric dipole approximations [10–12]. Here i indicates the polarization of the photon fields: $i = 1$ for R and $i = 2$ for L . j indicates the spin of the electron in the QD: $j = 1$ for up-spin and $j = 2$ for down-spin. d and d^\dagger are the annihilation and creation operator of the electrons in the QD ($dd^\dagger + d^\dagger d = 1$), and subscripts c and v indicate the conduction and the valence band ground states, respectively.

Hamiltonian (7) does not include the exciton-reservoir coupling. We assume that excitonic dipole decays with a phenomenological constant γ_{ex} due to the coupling to photon and phonon reservoirs. Assuming the cavity mirror does not change the polarization and following Gardiner and Collett [11], we approximate $\kappa_{ii'}(\omega) = \{\gamma_p/(2\pi)\}^{1/2} \delta_{ii'}$ and replace the reservoir field amplitude $b_i(\omega)$, $b_i^\dagger(\omega)$ with

$$a_i^{in}(t) = \frac{-1}{\sqrt{2\pi}} \int e^{-i\omega(t-t_0)} b_{0i}(\omega) d\omega,$$

$$a_i^{out}(t) = \frac{1}{\sqrt{2\pi}} \int e^{-i\omega(t-t_1)} b_{1i}(\omega) d\omega. \quad (9)$$

Here $b_{0i}(\omega)$ and $b_{1i}(\omega)$ are the values of $b_i(\omega)$ at $t = t_0$ and t_1 ($t_0 < t < t_1$), respectively.

After assuming the selection rule for the electric dipole transition, i.e., $\Omega_{ij} = \Omega_i \delta_{ij}$, the Heisenberg equations of motion for the amplitude of the fields are then,

$$\begin{cases} \frac{da_i}{dt} = -i\omega_p a_i - \frac{\gamma_p}{2} a_i - \frac{\Omega_i^*}{2} \sigma_i + \sqrt{\gamma_p} a_i^{in} \\ \frac{d\sigma_{-i}}{dt} = -i\omega_{ex} \sigma_{-i} - \frac{\gamma_{ex}}{2} \sigma_{-i} - \frac{\Omega_i}{2} \sigma_{zi} a_i \\ a_i^{out} = -a_i^{in} + \sqrt{\gamma_p} a_i \end{cases}. \quad (10)$$

Eqs.(10) consist of two independent sets corresponding to ($i = 1$: R , down-spin) and ($i = 2$: L , up-spin).

The frequency dependent response of the cavity system is obtained from Eq.(10) with linearization by using $\langle \sigma_{zi} \rangle$.

$$r_i(\omega) = \frac{a_i^{out}(\omega)}{a_i^{in}(\omega)} = -\frac{(\omega - \omega_p - i\frac{\gamma_p}{2})(\omega - \omega_{ex} + i\frac{\gamma_{ex}}{2}) - \frac{|\Omega_i|^2 \langle \sigma_{zi} \rangle}{4}}{(\omega - \omega_p + i\frac{\gamma_p}{2})(\omega - \omega_{ex} + i\frac{\gamma_{ex}}{2}) - \frac{|\Omega_i|^2 \langle \sigma_{zi} \rangle}{4}}. \quad (11)$$

When $\langle \sigma_{zi} \rangle = 0$, i.e., the conduction and valence band ground states of the same spin are both occupied or both empty, there is no effective coupling between the cavity photon and the QD exciton, and $r(\omega)$ is reduce to a cold cavity reflectance $r_0(\omega)$ [13];

$$r_0(\omega) = -\frac{(\omega - \omega_p - i\frac{\gamma_p}{2})}{(\omega - \omega_p + i\frac{\gamma_p}{2})}. \quad (12)$$

For the case where one valence electron exists with the spin state, we assume $\langle \sigma_{zi} \rangle \simeq -1$, that maximizes the optical Faraday effect. Hereafter, we omit the subscript i .

The solution (11) is reduced to

$$r(\omega) = -\frac{(\omega - \omega'_p(\omega) - i\frac{\gamma_p^-(\omega)}{2})}{(\omega - \omega'_p(\omega) + i\frac{\gamma_p^+(\omega)}{2})},$$

$$\begin{aligned}\omega'_p(\omega) &= \omega_p + \frac{\Omega^2}{4} \frac{\omega - \omega_p - \Delta}{(\omega - \omega_p - \Delta)^2 + \left(\frac{\gamma_{ex}}{2}\right)^2}, \\ \gamma_p^\pm(\omega) &= \gamma_p \pm \frac{\Omega^2}{4} \frac{\gamma_{ex}}{(\omega - \omega_p - \Delta)^2 + \left(\frac{\gamma_{ex}}{2}\right)^2}.\end{aligned}\quad (13)$$

where $\Delta \equiv \omega_{ex} - \omega_p$. In the limit of large detuning and probe frequency close to the cavity resonance, i.e., $\Delta \gg \gamma_{ex}/2, \Omega \gg \omega - \omega_p$, $\omega'_p(\omega)$ and $\gamma_p^\pm(\omega)$ become constant;

$$\omega'_p \simeq \omega_p - \frac{\Omega^2}{4\Delta}, \quad \gamma_p^\pm \simeq \gamma_p, \quad (14)$$

so that the response is the same as that of the empty cavity except for a finite frequency shift $d\omega_p = \Omega^2/(4\Delta)$.

Figure 2 shows the phase responses of the cavity for the empty and the coupled exciton-field cases. The detuning $\Delta = 400$ THz for the latter case. Other parameters are $\gamma_{ex} = 10$ GHz, $\omega_{ex} = 2.1 \times 10^{15}$ Hz, and $\gamma_p = 2$ THz ($Q = 10^3$). The vacuum Rabi frequency Ω is evaluated from the spontaneous emission decay rate formula $\gamma_{rad} = \omega^3 e^2 |r_{cv}|^2 n_0 / (3\pi\epsilon_0\hbar c^3)$ via

$$\Omega^2 = 4 \frac{e^2 |r_{cv}|^2}{3\hbar^2} \frac{\hbar\omega}{2\epsilon_0 n_0^2 V_{cav}} = \frac{2\pi c^3}{n_0^3 V_{cav} \omega_p^2} \gamma_{rad}. \quad (15)$$

Using an exciton radiative recombination rate $\gamma_{rad} = 2$ GHz, cavity volume $V_{cav} \sim (\lambda/n)^3 \sim 2 \times 10^{-2} (\mu\text{m})^3$, and $n_0 = 3.6$, Ω is estimated to be about 300GHz.

In Fig. 2, near the cavity resonance, the effect of exciton appears as the lateral shift of the response curve as mentioned above. The phase shift is given by

$$d\theta = d\omega_p \frac{4Q}{\omega_p} = \frac{\Omega^2}{\Delta\omega_p} Q. \quad (16)$$

This is the enhancement that we expect: if the cavity Q is large, the curve is steep and the phase difference becomes large.

IV. FEASIBILITY OF A QND MEASUREMENT

In this section, we discuss the feasibility of the QND measurement of a single electron spin. We impose four conditions for the QND measurement for this system: (A) an expected signal is larger than the shot noise, (B) real excitation of the QD exciton is negligible during the measurement, (C) integration time of the measurement is longer than the cavity lifetime, and then (D) spin lifetime of a QD is longer than the integration time. We will derive conditions (A)-(C) and discuss the region where the solutions exist, and then compare it with condition (D).

For the polarization-sensitive interferometer with a balanced homodyne detector in Fig. 3, the signal is

$$|A_y| = \sin\left(\frac{d\theta}{2}\right) \bar{r} |A_{in}|, \quad (17)$$

where $|A_{in}|^2 = N_{in}$ is normalized to the incident photon flux of the probe. If the probe power and the local oscillator power are equal, the signal (normalized to photon flux) due to the single electron spin N_{SS} is

$$N_{SS} = N_{in} \sin\left(\frac{d\theta}{2}\right) \bar{r}. \quad (18)$$

The standard quantum limit (SQL) N_{SQL} for the homodyne detection is given by

$$N_{SQL} = \sqrt{\frac{N_{in}}{\tau}}, \quad (19)$$

where τ is the integration time. The SQL originates from the vacuum fluctuation in the p-polarization incident from the open port of the polarization beam splitter (PBS) of Fig.3. In order to observe the single spin effect, the signal N_{SS} must be greater than N_{SQL} , which leads to condition (A):

$$N_{in}\tau > \left(|r| \sin \left(\frac{d\theta}{2} \right) \right)^{-2}, \quad (20)$$

which places a lower bound for the number of photons used in the measurement.

Condition (B) is expressed by

$$(1 - |r|^2)N_{in}\tau < 1, \quad (21)$$

which places an upper bound for the number of photons used during the measurement.

With condition (C) $\tau > 1/\gamma_p$, the region where the solutions exist is shown in Fig. 5. Three curves are plotted, in Fig.5(a), as a function of normalized detuning, using $P = \hbar\omega N_{in} = 10\text{mW}$, $\omega = 2.1 \times 10^{15}\text{Hz}$, and $\gamma_p = 0.1\Omega^2/(4\gamma_{ex}) = 230\text{GHz}(Q \sim 10^4)$. The hatched region (top right part) is where the solutions exist. Figure.5(b) shows the similar result but γ_p is set equal to $\Omega^2/(4\gamma_{ex}) = 2.3\text{THz}(Q \sim 10^3)$. The curves (A) and (B) coincide with each other and this is the limit for the solutions to exist: if $\gamma_p > \Omega^2/(4\gamma_{ex})$, there is no solution. We see that the detuning $\Delta/(\gamma_{ex}/2)$ must be much larger than 1, in this case $\sim 10^3$, for the system to have a solution.

Figure 6 shows the integration time necessary for the measurement under the large detuning, as a function of cavity Q value. The expectation value $\langle n_{ex} \rangle = \langle \sigma_+ \sigma_- \rangle$ is used as a parameter, since it expresses the fundamental limit $\langle n_{ex} \rangle \ll 1$ corresponding to the approximation $\langle \sigma_z \rangle \simeq -1$ appeared in Sec. III. With the large detuning, $\langle n_{ex} \rangle$ is derived from Eq.(10);

$$\begin{aligned} \langle n_{ex} \rangle &= \frac{\Omega^2}{4\Delta^2} \langle a^\dagger a \rangle \\ &= \frac{\Omega^2 Q}{\Delta^2 \omega_p} \langle a^{in\dagger} a^{in} \rangle = \frac{\Omega^2 Q}{\Delta^2 \omega_p} N_{in}. \end{aligned} \quad (22)$$

Using Eqs.(22) and (16), conditions (A)-(C) are

$$\tau > \frac{4\omega_p}{\Omega^2} \frac{1}{\langle n_{ex} \rangle} \frac{1}{Q}, \quad (23)$$

$$\tau < \frac{1}{\gamma_{ex} \langle n_{ex} \rangle}, \quad (24)$$

$$\tau > \frac{1}{\omega_p} Q, \quad (25)$$

respectively. Eq.(24) reveals that the real excitation rate is the product of the expectation value of the exciton number and the exciton's dephasing rate. In Fig.6, the vertical solid line is the limit $\gamma_p = \Omega^2/(4\gamma_{ex})$ discussed above. The QND conditions are satisfied only in the right of this vertical line. Another solid line expresses Eq.(25). Three combinations of Eqs.(23), (24), and (25) are shown in the figure with the parameter $\langle n_{ex} \rangle$ set to 0.1, 0.01, and 0.001, and corresponding three triangular regions are seen with heavy hatching. Lightly hatched part is the total region where the solutions exist. We see that in order to achieve the QND measurement, we need cavity Q of $10^3 \sim 10^4$ and integration time of about 100ps~10ns.

Since spin lifetime of a doped-QD exciton is expected to be longer than 100ns [2,6], the integration time we derived is encouraging to perform the QND measurement. It is also suggested that a reasonably high- Q cavities, which are within the reach of experimental microcavity and photonic bandgap structure, can meet the requirements.

V. CONCLUSION

We have formulated the response of optical cavity with a single QD using Langevin equations including both QD exciton and external probe field. The signal to noise ratio in detecting the spin is evaluated. We conclude that the QND measurement for a single electron spin in a doped-QD can be achieved by the proposed scheme with a reasonably high- Q cavity under large detuning condition.

* Visiting Researcher for 1999-2001 and also with Canon Inc. Present address: Optical Technology Research Center, Canon Inc., 23-10 Kiyohara-Kogyodanchi, Utsunomiya, Tochigi, Japan 321-3231. E-mail: sugita.mitsuro@canon.co.jp,

- [1] D. Loss and D. P. DiVincenzo, Phys. Rev. A **57**, 120 (1998).
- [2] A. Imamoglu, D. D. Awschalom, G. Burkard, D. P. DiVincenzo, D. Loss, M. Sherwin, and A. Small, Phys. Rev. Lett. **83**, 4204 (1999).
- [3] W. Heller and U. Bockelmann, Phys. Rev. B **55**, 4871 (1996).
- [4] Y. Toda, S. Shinomori, K. Suzuki and Y. Arakawa, Phys. Rev. B **58**, 10147 (1998).
- [5] J. M. Kikkawa, I. P. Smorchkova, N. Samarth and D. D. Awschalom, Science **277**, 1284 (1997).
- [6] J. M. Kikkawa and D. D. Awschalom, Phys. Rev. Lett. **80**, 4313 (1998).
- [7] J. A. Gupta, D. D. Awschalom, X. Peng and A. P. Alivisatos, Phys. Rev. B. **59**, 10421 (1999).
- [8] G. S. Solomon, M. Pelton and Y. Yamamoto, Phys. Rev. Lett. **86**, 3903 (2001).
- [9] M. Pelton, Y. Yamamoto, J. Vuckovic and A. Scherer, submitted for publication.
- [10] F. W. Cummings, Phys. Rev. **140**, A105 (1965).
- [11] C. W. Gardiner and M. J. Collett, Phys. Rev. A **31**, 3761 (1985).
- [12] S. Pau et al., Phys. Rev. B **51**, 14437 (1995).
- [13] D. F. Walls and G. J. Milburn, *Quantum Optics*, 121 (Springer-Verlag, Berlin, 1994).
- [14] S. Bar-Ad and I. Bar-Joseph, Phys. Rev. Lett. **68**, 349 (1992).
- [15] T. C. Damen, Karl Leo, Jagdeep Shah, and J. E. Cunningham, Appl. Phys. Lett. **58**, 1902 (1991).
- [16] H. Gotoh et al., Appl. Phys. Lett. **72**, 1341 (1998).
- [17] V. K. Kalevich et al., Physics of the Solid State **41**, 789 (1999).

FIG. 1. Sample and its electronic states. (a) Sample: a single QD in a micropost semiconductor cavity. Three dimensional confinement is due to the micropost structure and multilayer Bragg mirrors. The Bragg mirror consists of $\lambda/4$ thick AlGaAs and AlAs layers. An InAs-QD is embedded in a GaAs cavity. (b),(c) Electronic state configurations of the QD, coupling with probe fields: c and v indicate conduction and valence band ground states of the QD. Arrows are for the spin states. Filled states are with black dots, empty states are with white. R and L denote circular polarizations of the probe fields, which interact with electron excitation (indicated by x's) obeying the selection rule. r_R and r_L are the reflectivities.

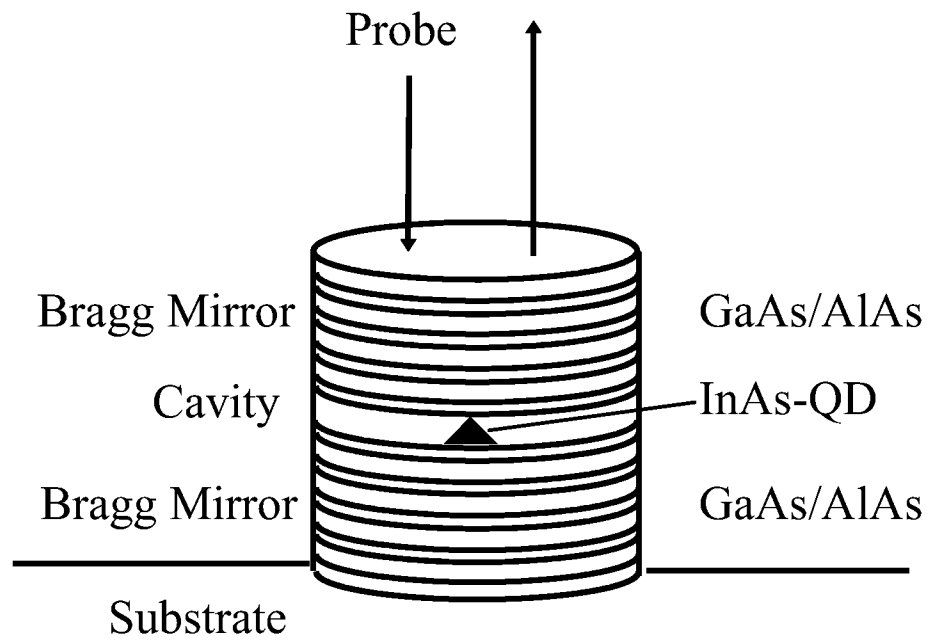
FIG. 2. Phase response of the cavity with and without coupling to the QD exciton. (a) Two curves are not distinguished in this scale. A cold cavity is in phase on the resonance $\omega = \omega_p$, and out of phase off the resonance. (b) Near the cavity resonance. QD exciton effect appears as a shift of the resonant frequency by $d\omega_p$.

FIG. 3. Proposed experimental setup. Essential elements of the interferometer. Laser beam is prepared as 45 degree linear polarization (not shown). It is divided into p-polarization (for local) and s-polarization (for signal) by the first polarizing beam splitter (PBS). After reflected by the sample, signal polarization is rotated by the optical Faraday effect to have p-polarization (dp in the figure). From the reflected signal light, s-polarization is removed by the second PBS and the residual dp is mixed by the beam splitter (BS). The interference between local and signal light is detected by a balanced homodyne detector.

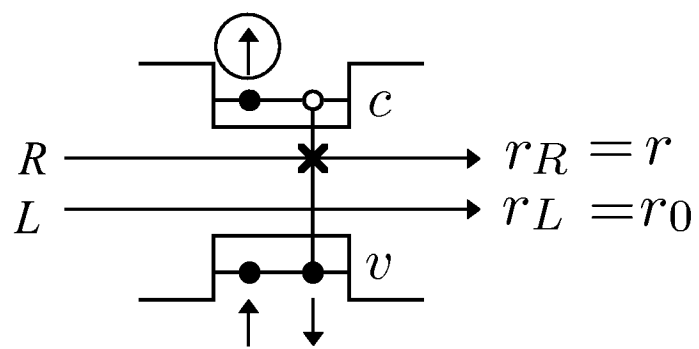
FIG. 4. Fields and couplings of the system. a for the cavity photon, σ for the QD exciton, and a^{in} and a^{out} for the probe photon. The probe photons are coupled with cavity photons by γ_p the coupling and dissipation constant. The QD excitons are coupled with the cavity photons by the Rabi Frequency Ω , and with the non-cavity modes with dissipation constant γ_{ex} .

FIG. 5. Conditions for the measurement photon number and the detuning. Condition (A): the shot noise limitation (solid line) and condition (B): the real excitation limitation (dotted line) have their corner points at the detuning close to the exciton dissipation $\gamma_{ex}/2$. Condition (C): the integration time limitation is constant. In (a), the area satisfying all the conditions is hatched (top right). In (b), conditions (A) and (B) shares the line and the satisfied area is critical.

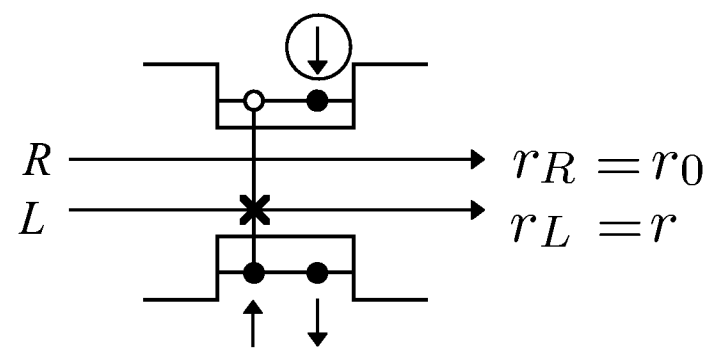
FIG. 6. Conditions for measurement time and cavity Q. In the legend, the lines used for conditions (A) and (B) with parameter $\langle n_{ex} \rangle$ are displayed. Condition (B) appears as horizontal lines. Condition (C) (solid line from bottom left to top right) and a combination of conditions (A) and (B) enclose a triangle (dark hatched), which is the region the solutions exist. The vertical line shows $\gamma_p > \Omega^2/(2\gamma_{ex})$, which the top left apex of the triangular region traces as $\langle n_{ex} \rangle$ changes.



(a)



(b)



(c)

Fig. 1

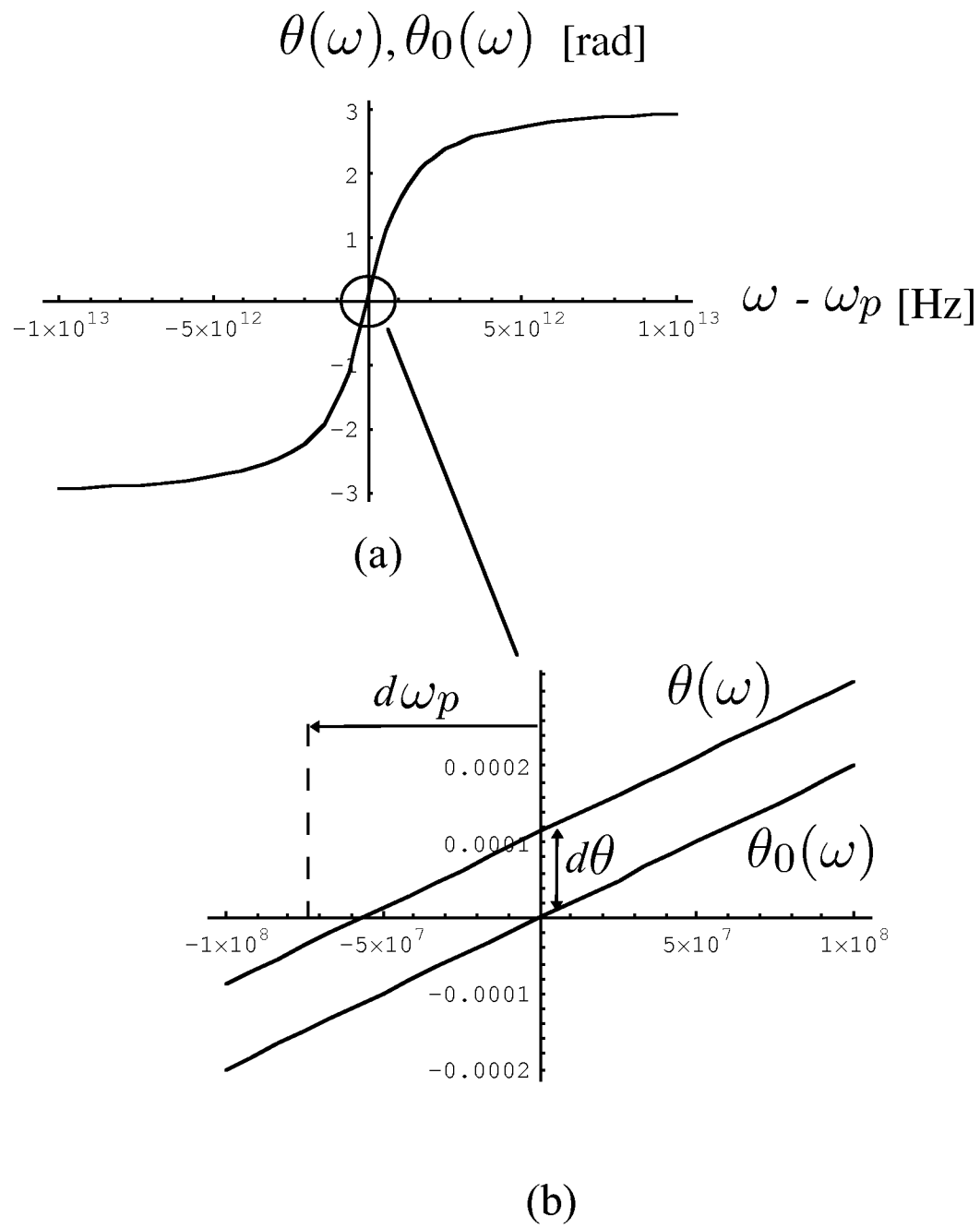


Fig. 2

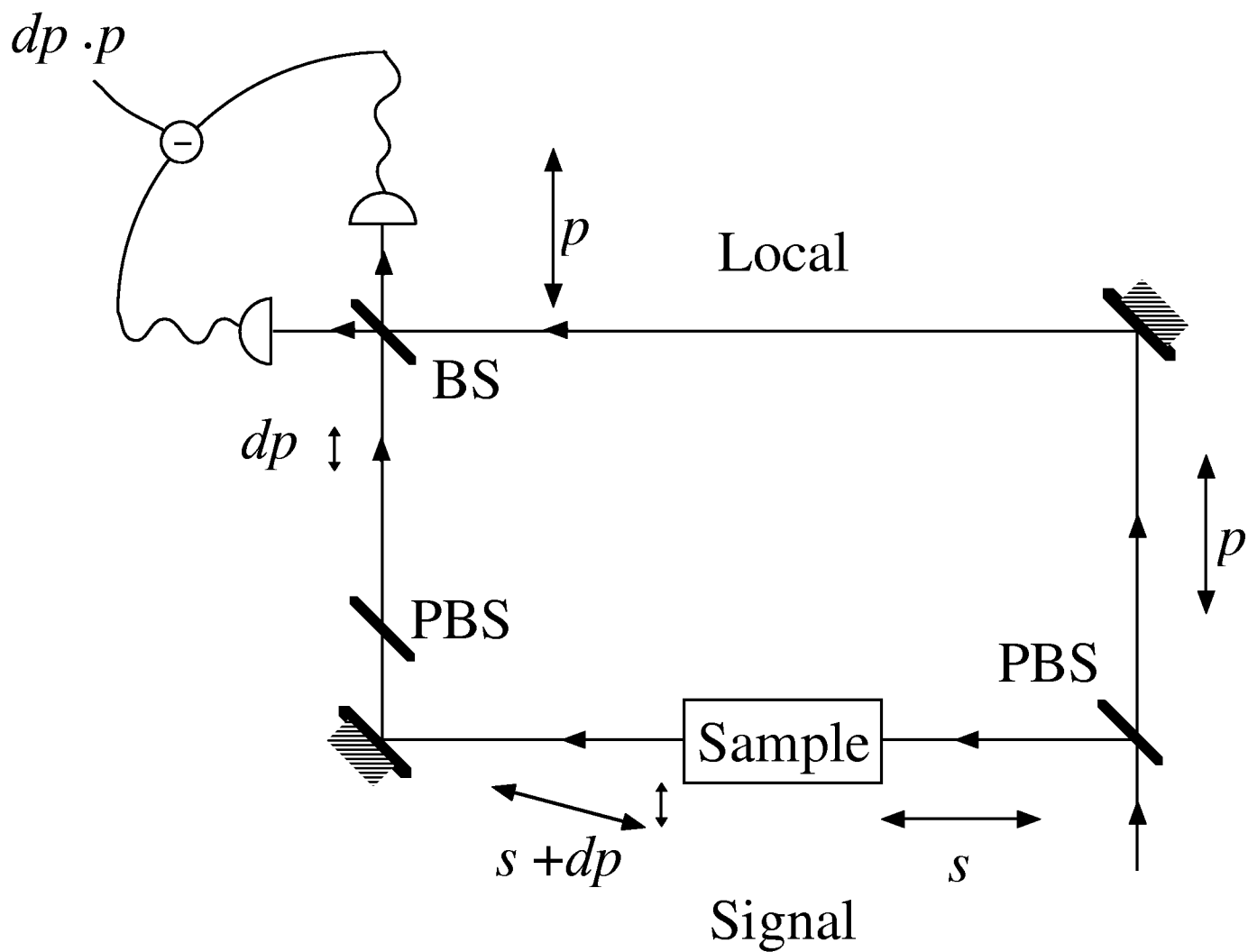


Fig. 3

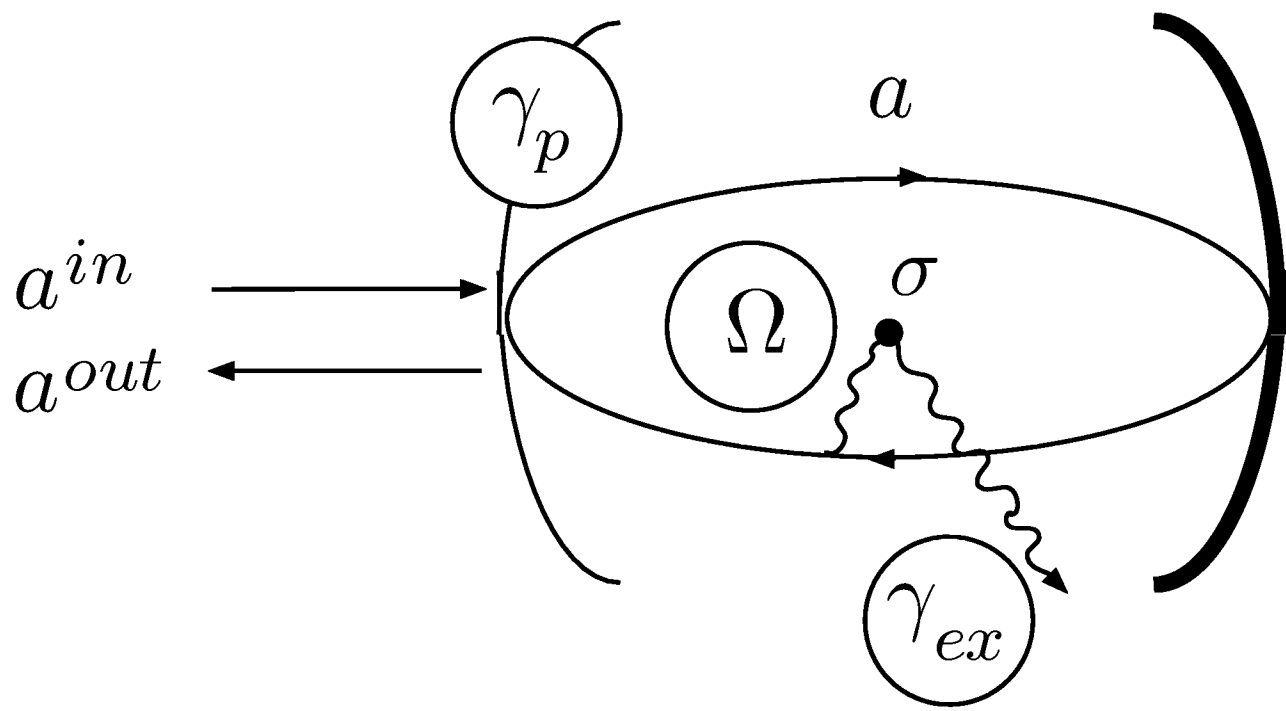
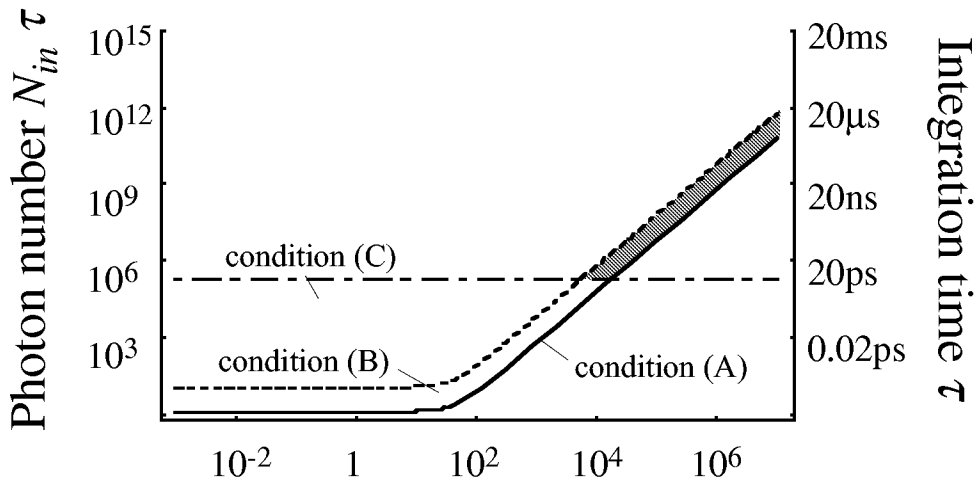
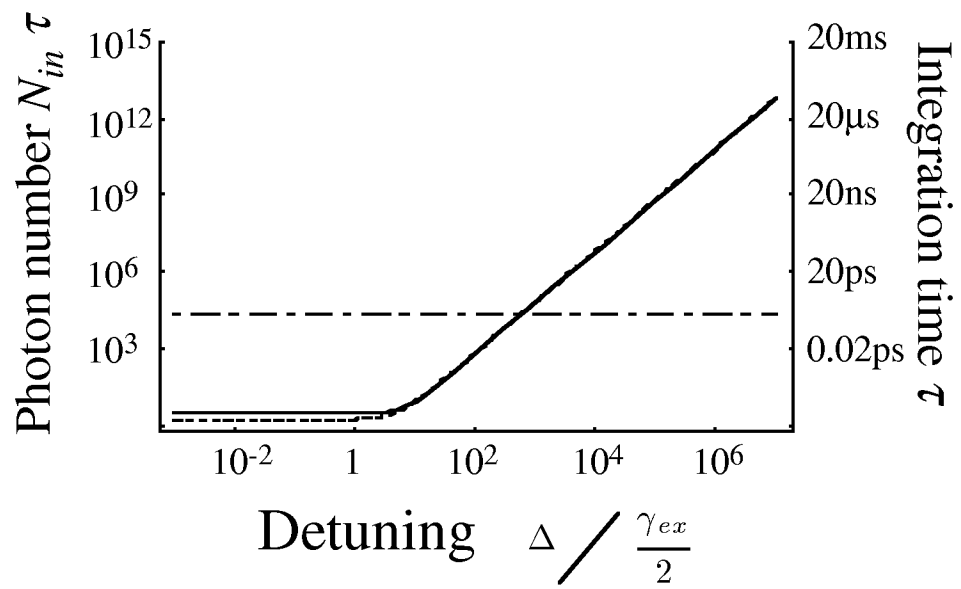


Fig. 4



(a)



(b)

Fig. 5

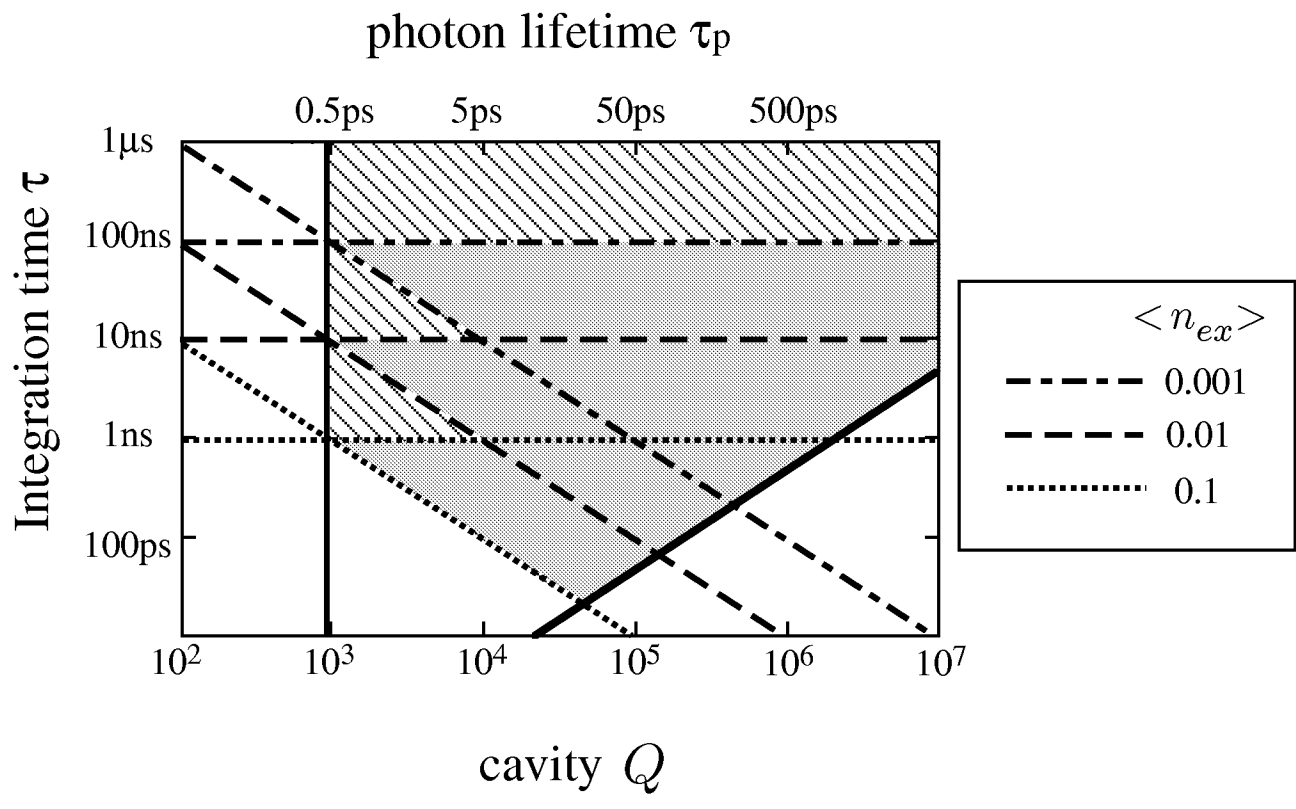


Fig. 6